Published in final edited form as:
J Neural Eng. 2011 February ; 8(1): 016007. doi:10.1088/1741-2560/8/1/016007.

Electric field strength and focality in electroconvulsive therapy and magnetic seizure therapy: A finite element simulation study

Zhi-De Deng[1,2], **Sarah H. Lisanby**[3,1], and **Angel V. Peterchev**[1,*]

Zhi-De Deng: zd2119@columbia.edu; Sarah H. Lisanby: sarah.lisanby@duke.edu; Angel V. Peterchev: ap2394@columbia.edu

[1]Division of Brain Stimulation and Therapeutic Modulation, Department of Psychiatry, ColumbiaUniversity/New York State Psychiatric Institute, 1051 Riverside Drive, Unit 21, New York, NY 10032, USA

[2]Department of Electrical Engineering, Columbia University, 1300 S. W. Mudd, 500 West 120th Street, New York, NY 10027, USA

[3]Department of Psychiatry and Behavioral Sciences, Duke University, Box 3950 DUMC, Durham, NC27710, USA

Abstract

We present the first computational study comparing the electric field induced by various electroconvulsive therapy (ECT) and magnetic seizure therapy (MST) paradigms. Four ECT electrode configurations (bilateral, bifrontal, right unilateral, and focal electrically administered seizure therapy) and three MST coil configurations (circular, cap, and double cone) were modeled. The model incorporated a modality-specific neural activation threshold. ECT (0.3 ms pulse width) and MST induced maximum electric field in the brain of 2.1–2.5 V/cm and 1.1–2.2 V/cm, corresponding to 6.2–7.2 times and 1.2–2.3 times the neural activation threshold, respectively. The MST electric field is more confined to the superficial cortex compared to ECT. The brain volume stimulated was much higher with ECT (up to 100%) than MST (up to 8.2%). MST with the double cone coil was the most focal and bilateral ECT was the least focal. Our results suggest a possible biophysical explanation of the reduced side effects of MST compared to ECT. Our results also indicate that the conventional ECT pulse amplitude (800–900 mA) is much higher than necessary for seizure induction. Reducing the ECT pulse amplitude should be explored as a potential means of diminishing side effects.

1. Introduction

Electroconvulsive therapy (ECT) remains a widely used treatment for severe depression because its antidepressant efficacy and speed of response are unsurpassed by other interventions. However, ECT carries a risk of significant cognitive side effects [1] and cardiac complications [2]. Over the last few decades, the tolerability of ECT has been improved by altering the electrode placement and the pulse train parameters, as exemplified by the transition from bilateral (BL) to right unilateral (RUL) electrode placement [3] and the transition from sinusoidal to brief [4, 5] and, more recently, to ultra-brief pulses [6]. In addition, alternative electrode configurations that are intended to target prefrontal structures, such as bifrontal (BF) [7] and focal electrically administered seizure therapy (FEAST) [8], are being evaluated. Finally, magnetic seizure therapy (MST), in which seizures are induced using repetitive transcranial magnetic stimulation (rTMS), has been introduced in an effort

*Corresponding author: Columbia University, Department of Psychiatry, 1051 Riverside Drive, Unit 21, tel. 1-212-543-5460, fax. 1-212-543-4340, ap2394@columbia.edu.

to improve the risk/benefit ratio of convulsive therapy, as it offers greater control of the seizure initiation site and a superior side effect profile than conventional ECT [9].

Despite the evidence that the stimulation parameters have an impact on efficacy and side effects, unanswered questions remain regarding the mechanisms by which variations in treatment technique lead to differences in clinical outcome [10, 11]. The strength and spatial distribution of the electric field induced by ECT and MST determines the extent to which various brain regions are directly affected by the stimulation. Knowledge of this distribution may help to explain differences in efficacy and side effects seen with existing paradigms and may inform novel methods to improve spatial targeting of seizure therapies as well as subconvulsive electrical and magnetic stimulation. However, since there are no established non-invasive methods for measuring the electric field induced in the human head by ECT, there are scare experimental data and they are limited to cadaver preparations. Smitt and Wegener measured the intracerebral voltage distribution in human cadavers during ECT using probes progressively passing through the brain from the occipital protuberance to the supraorbital ridge [12]. Lorimer et al. carried out intracerebral voltage measurements in human cadavers with bifrontotemporal and vertex– parietal electrode placements [13]. Rush and Driscoll measured the voltage distribution in an electrolytic tank containing a human half skull and found that the estimated current density agrees well with a computational model consisting of three concentric spherical shells representing the scalp, skull, and brain [14]. There is one study to date reporting on the direct intracranial measurements of TMS-induced electric field in the human cortex—using a figure-8 coil, Wagner et al. recorded the TMS-induced voltages between 5 mm-spaced contacts on an implanted electrode within the right cingulate [15]. Finally, intracerebral induced voltages have been recorded with implanted electrodes in spider monkeys for ECT [16] and in rhesus monkeys for ECT and MST [17]; however, the difference in head size and structure limits the generalizability to human subjects [18, 19]. Although these *ex vivo* and *in vivo* measurements in human and non-human primate heads provide insights and are important for validating computational models, they provide estimates of the electric field at sparse locations in the brain and are not available for the full range of electrode and coil configurations used clinically. Therefore, computational models are necessary for the detailed study of the intracerebral electric field induced by ECT and MST.

A number of theoretical and computational analyses of the electric field induced by ECT have been presented for spherical [20-23] and anatomically realistic head models [24-29]. These studies, however, have various limitations, including representing the electrodes as point sources, truncated or 2D head models, and models limited to the BL and RUL electrode placements. Except for a recent study by our group [29], none of these works has modeled the BF and FEAST electrode configurations. Further, even though a significant number of papers on TMS electric field modeling have been published [24-26, 30-36], none of them analyzes MST-specific devices and coils.

The published studies have one more common limitation: Knowing the electric field distribution alone is not sufficient to predict the strength of neural stimulation, since neural response depends also on the pulse shape and width. The dependence on pulse width is often expressed as a strength-duration relation [37]. Therefore, in addition to characterizing the maximum induced electric field, we propose that the more appropriate metric to quantify the strength of stimulation is the electric field amplitude relative to the threshold electric field for neural activation. The electric field threshold accounts for pulse characteristics such as pulse shape and width, and can be obtained empirically. Existing simulation studies comparing ECT and TMS do not incorporate these aspects of the neural response to the induced electric field. Thus, those studies cannot reveal the spatial extent of direct brain activation and do not allow appropriate comparison between stimulation with different pulse

characteristics, such as between the rectangular pulse waveforms of ECT and the sinusoidal waveforms of MST.

This is the first computational study to compare the electric field strength and focality of ECT and MST configurations. In addition, we derive a method for estimating the electric field threshold for neural activation for various stimulation pulse shapes and widths based on data from the literature. The estimated neuronal activation threshold is incorporated into our models to determine the strength and focality of direct neural stimulation by ECT and MST. The comparison of the stimulation strength and focality of various existing forms of ECT and MST may inform the interpretation of clinical data on the differences between these modalities, and could be useful in guiding improvements in ECT and MST dosing. This work was previously presented in part in conference publications [19, 38].

2. Materials and methods

2.1. Electric field simulation

We simulated the electric field induced by commercial ECT and MST devices: MECTA Spectrum 5000Q (MECTA Corp., Tualatin, OR) and Magstim Theta (Magstim Co., Whitland, Wales, UK), respectively. The spatial distribution of the electric field induced in a spherical head model for various ECT electrode and MST coil configurations was simulated using the finite element method (FEM) with the software packages ElecNet 7 and MagNet 7 (Infolytica Corp., Montreal, Canada), respectively. In FEM, the head and the ECT electrodes and MST coils are represented as 3D objects meshed into small contiguous tetrahedrons (finite elements) that are assigned dielectric properties corresponding to the respective tissues and materials. The electric field temporal waveforms were directly measured from the output of the ECT and MST devices. The electric field modeling approach is detailed below.

2.1.1. Head model and anatomical parameters—The human head was modeled as a five-shell conducting sphere consisting of scalp, skull, cerebrospinal fluid, gray matter, and white matter, as shown in figure 1(h). Even though the spherical model substantially simplifies the head geometry, it has been validated with *in vivo* voltage measurements during electrical stimulation [12-14] and provides a reasonable approximation to anatomically realistic models of TMS [36]. Thus, the spherical model provides a useful platform for studying transcranial bran stimulation. Since about 70% of ECT patients are women [39], we used the weighted average of adult female head diameter [40, 41], and scalp thickness [42, 43] reported in morphometric studies. The skull thickness of the head model was based on averaging the frontal, parietal and occipital bone measurements reported by Li et al. [44]. The tissue layer thicknesses used in the model are summarized in table 1. The edges of each tetrahedron in the finite element mesh were constrained to be less than 2.5 mm; the complete mesh consisted of approximately 1.8 million finite elements.

The tissue layers were assigned the isotropic conductivities given in table 1 [14, 34, 45-48]. We used tissue conductivities that are independent of frequency; this assumption is justifiable at the relatively low frequencies comprising ECT and MST pulses (< 10 kHz) [34, 36, 45-47, 49, 50]. Traditionally, a brain-to-skull conductivity ratio of 80 has been most commonly used in modeling studies [51, 52]. However, more recent *in vivo* measurements have indicated that this ratio is in the range of 15–40 [53-56]. Some sophisticated skull models have incorporated multi-layer structure and/or anisotropy [57]; however, boundaries between the spongiosa and the compacta layers of the skull are often difficult to determine on MRI scans [48, 57]. Therefore, in this study we modeled the skull as a single layer, with a gray-matter-to-skull conductivity ratio of 40 [53].

2.1.2. ECT electrode and MST coil configurations—Four ECT electrode configurations (BL, BF, RUL, and FEAST) and three MST coil configurations [circular (CIRC), cap (CAP), and double cone (DCONE)] were modeled after existing hardware. The electrode and coil placements approximated those used in clinical practice (or in clinical trials, in the case of FEAST and MST) mapped onto the surface of the spherical model. Standard round, 5 cm diameter electrodes were modeled in the BL, BF, and RUL configurations. For BL ECT [figure 1(a)] the two electrodes were placed in the frontotemporal position— the bottom of the electrodes tangential to the midpoint of the line connecting the auditory meatus and the external canthus of the eye [58]. For BF ECT [figure 1(b)] each electrode was centered 5 cm above the outer angle of the orbit on a line parallel to the sagittal plane [7]. For RUL ECT [figure 1(c)] one electrode was placed in the right frontotemporal position and the second electrode was placed 2.5 cm to the right of vertex [58]. The FEAST [figure 1(d)] electrode configuration consisted of a large rectangular electrode pad (2.5 cm × 6.3 cm) over the right motor strip and a small circular electrode (2 cm diameter) over the right eyebrow [8]. Since the sphere is rotationally invariant, the ECT electrode placements in the model were determined by approximating the edge-to-edge inter-electrode spacing for each configuration: BL, 13 cm; RUL and BF, 4 cm; and FEAST, 9 cm. For the same reason, the position and orientation of the MST coils did not matter for the metrics we computed.

The MST coils were modeled after commercial coils from Magstim Co. using manufacturer's data, X-rays, and inductance measurements to reproduce their structure and electrical characteristics. The CIRC coil (S/N MP39) consisted of two parallel layers of windings connected in series, each with an inner diameter of 44 mm, outer diameter of 120 mm, and 9 turns [figure 1(e)]. The CAP coil (P/N 8985) consisted of a single-layer, concave circular winding with inner diameter of 68 mm, outer diameter of 130 mm, and 15 turns [figure 1(f)]. The DCONE coil (S/N MP40) consisted of two adjacent windings fixed at a relative angle of 120°, each with an inner diameter of 96 mm, outer diameter of 125 mm, and 7 turns [figure 1(g)]. The coil windings were modeled as solid copper wires with cross-sectional dimensions of 6 mm × 1.75 mm. The coil conductors were placed 7 mm from the surface of the head model to account for the thickness of the insulating coil casing.

2.1.3. Electric field solution—Since ECT and MST induce electric fields of relatively low frequencies (< 10 kHz), the quasistatic approximation can be deployed in electric field models [36, 50, 59-61]. Under the quasistatic approximation, the electric field solution can be expressed as the product of a spatial factor, $k(\mathbf{r})$, and a time-domain pulse waveform for the ECT electrode current $I_E(t)$ or the MST coil voltage $V_M(t)$

$$E(\mathbf{r},t)=\begin{cases} k_E(\mathbf{r})I_E(t)=k_E(\mathbf{r})I_{E0}w_E(t)=E_E(\mathbf{r})w_E(t), \text{ for ECT} \\ k_M(\mathbf{r})V_M(t)=k_M(\mathbf{r})V_{M0}w_M(t)=E_M(\mathbf{r})w_M(t), \text{ for MST} \end{cases} \quad (1)$$

where $\mathbf{r}$ is the spatial coordinate vector, t is time, I_{E0} and V_{M0} are the peak ECT electrode current and MST coil voltage, and $w_E(t)$ and $w_M(t)$ are the ECT and MST unit-amplitude pulse waveforms (see figure 2), respectively. The static electric field amplitude distribution in space, $E(\mathbf{r})$, is directly proportional to the peak ECT electrode current I_{E0} or MST coil voltage V_{M0}, and to the geometric factor $k(\mathbf{r})$ which depends on the electrode or coil geometry and placement as well as on the head geometry and dielectric properties. The ECT electric field spatial distribution, $E_E(\mathbf{r})$, was computed for a direct current of 800 mA (corresponding to the conventional MECTA output setting) using the ElectNet 3D Current Flow solver. ElecNet and MagNet solve for the magnetic field via the edge-element version of the T-Ω method [62] and then compute the electric field from the magnetic field [63]. The

ECT waveform was recorded from a MECTA Spectrum 5000Q set to current amplitude of 800 mA and pulse widths of 0.3 ms and 1 ms, with the electrodes connected to a 300 Ω resistive load. The normalized waveform, $w_E(t)$, was obtained by dividing the electrode current by its peak value [see figure 2(a) for a representative waveform]. Whereas ultra-brief pulses (0.3 ms) are now common in RUL ECT, brief pulses (1 ms) are still standard in BL ECT due to inefficacy of ultra-brief pulse BL ECT with conventional dosing [6].

The MST spatial electric field distribution was first computed for an arbitrary coil current I_{M0} = 1 A and frequency $\omega_0 = 2\pi\times5$ kHz using the MagNet Time Harmonic solver, yielding a distribution with unadjusted amplitude, $E'_M(\mathbf{r})$. The electric field was then scaled to match the output of a Magstim Theta device

$$E_M(\mathbf{r}) = E'_M(\mathbf{r})\frac{V_C}{I_{M0}\omega_0 L} \quad (2)$$

where V_C = 1.65 kV is the nominal energy-storage capacitor voltage at maximum pulse amplitude of the Magstim Theta and L is the coil inductance. The MST electric field waveform, $w_M(t)$, was recorded with a search coil from the Magstim Theta stimulator with each of the three modeled MST coils and then normalized to unit amplitude [see figure 2(b) for a representative waveform]. The simulation results were validated by measurement of the electric field induced by DCONE MST in a spherical head phantom (see Supplementary data).

2.2. Electric field characterization

The interaction of electric fields and cerebral neurons has not been fully characterized. For long, straight nerves, the spatial gradient of the electric field along the axon has been proposed to determine the degree of induced neuronal depolarization [64, 65]. However, theoretical analysis and *in vitro* experiments have shown that even in a uniform electric field, a large effective electric field gradient can occur at the terminations, bends, branches, or other nonuniformities in the axon [66-69]. Furthermore, induced electric field transverse to the axon can also cause neuronal depolarization [70]. Therefore, since the cerebral axons are short and/or bent, and since the transcranially induced electric field has a relatively small spatial gradient, strongest depolarization is likely to occur at the site of maximum electric field magnitude [71, 72]. This view is supported by comparisons of TMS activation maps with neuroimaging and direct cortical stimulation results [73-75]. Therefore, in this study we characterize the induced electric field strength as a predictor of direct neural activation.

2.2.1. Stimulation strength—To assess the degree of direct neural stimulation, the electric field strength has to be compared to a neural activation threshold. This threshold electric field can be estimated empirically. For example, the average threshold electric field in motor cortex to induce muscle response (the motor threshold) is 0.85 V/cm (range 0.3–1.3 V/cm) for the Magstim 200 TMS stimulator with a 70 mm figure-8 coil [76-79]. Since it can be easily quantified by electromyography, the motor threshold is used extensively in TMS as a probe of neural excitability. The TMS motor threshold data are in substantial agreement with measurements in anesthetized humans receiving transcranial electric stimulation where motor thresholds of 170–420 mA (correspond to electric field strengths of 0.45–1.12 V/cm) for 0.05 ms pulse width were reported [80]. Stimulation at 40% above the motor threshold produces robust neural activation with motor evoked potential amplitude of approximately 90% of maximum [81], indicating recruitment of the majority of the local neuronal population. Therefore, we will use the electric field corresponding to 1.4 × motor threshold as an approximate threshold for robust neural activation, E_{th}.

The empirically derived thresholds are specific to the pulse shapes and widths of the respective stimulation device. To estimate the corresponding electric field thresholds for other pulse shapes and widths, we have to consider a model of the neuronal membrane response to stimulation. For modeling of the neural firing threshold in transcranial stimulation, the neuronal membrane can be approximated as a low-pass filter with time constant τ_m [82-84]. Therefore, the change in membrane potential resulting from an electric field pulse, $E(\mathbf{r},t) = E(\mathbf{r})w(t)$, is approximately

$$\Delta V_{\mathrm{m}}(\mathbf{r},t)=\gamma E(\mathbf{r})(w*h)(t) \quad (3)$$

where '*' is the convolution operator and $h(t)$ is the impulse response of a low-pass filter with time constant τ_m

$$h(t)=\frac{1}{\tau_m}e^{-t/\tau_m}u(t) \quad (4)$$

where $u(t)$ is the Heaviside step function. It is thought that the axon is the neural element preferentially depolarized by extracellular electric field stimulation, corresponding to a membrane time constant of approximately τ_m = 150 μs [82, 85, 86]. Thus, $(w * h)(t)$ is proportional to the axonal membrane depolarization; it is plotted with dashed line in figure 2 together with the corresponding $w(t)$ for an ECT and an MST pulse.

The constant γ characterizes the membrane depolarization sensitivity to the electric field. The depolarization sensitivity may vary depending on the neuronal type and relative orientation to the electric field [87]. However, it is reasonable to expect that pyramidal neurons and interneurons that are depolarized by electric field of magnitude E_{th} in the motor cortex will have similar response to electric field in other brain areas. For example, TMS evoked electroencephalographic responses in motor and prefrontal cortices have been found to correlate [88, 89]. There is a 35% intrainidividual variation in motor threshold depending on coil orientation [90], which is comparable to interindividual threshold variability [81] and which may average out among the spread of neuronal orientations in a brain region (see also discussion in section 4.3).

Regardless of the pulse shape, the neuron will fire when ΔV_{m} reaches an approximately constant threshold level. Therefore, by equating ΔV_{m} at threshold for two pulse shapes, $w_1(t)$ and $w_2(t)$, we obtain the following relationship between the corresponding threshold electric field amplitudes

$$\frac{E_{\mathrm{th1}}}{E_{\mathrm{th2}}}=\frac{\max\left(|(w_2*h)(t)|\right)}{\max\left(|(w_1*h)(t)|\right)}. \quad (5)$$

Note that this result is independent of γ and the neural membrane firing threshold. From (5) and known electric field thresholds such as those reported for the figure-8 coil and the Magstim 200 stimulator, we can estimate the electric field thresholds for other ECT and MST pulse waveforms.

In the above analysis, we modeled the neural membrane response for single pulses, whereas ECT and MST are administered at pulse train frequencies of 20–240 pulses per second and 50–100 pulses per second, respectively. Modeling the neural membrane response to each stimulus train pulse as a single pulse response is justified as follows. Each MST pulse is charge balanced, so there is no significant membrane charge accumulation between pulses.

Individual ECT pulses are unidirectional but they alternate in polarity [11, 91]; thus, each ECT pulse pair is charge balanced and there is no cumulative charge injection. Furthermore, even for stimulus trains with unbalanced charge (e.g., a unidirectional pulse train [92]), the axonal membrane time constant ($\sim 150\ \mu s$) is short compared to the interpulse interval (> 3 ms), and, thus, the axonal membrane charge accumulation is negligible.

2.2.2. Stimulation focality—To characterize the superficiality of stimulation, we computed the maximum electric field strength as a function of depth from the brain surface. We quantified the volume of the brain directly activated by ECT and MST by the percentage of brain (gray and white matter) volume that is exposed to an electric field strong enough to produce suprathreshold depolarization in the majority of neurons, Vol ($E \geq E_{th}$). Further, we quantified the intrinsic focality of each electrode or coil configuration by the percentage of brain volume that is exposed to an electric field larger than the half-maximum electric field, Vol($E \geq E_{max}/2$) [72]. Unlike the directly activated brain volume, which changes with stimulus pulse shape, width, and amplitude, the intrinsic focality depends only on the electrode and coil geometry and placement, and is independent of the pulse waveform parameters.

3. Results

3.1. Electric field characterization

The electric field thresholds for robust neural activation for the various stimulation modalities were estimated using (5) and data linking motor threshold to the induced electric field [76-78]. Table 2 summarizes the data for the estimated neural membrane depolarization factor, $\max(|(w * h)(t)|)$, and neural activation threshold, E_{th}. Notably, E_{th} is approximately three times higher for MST than for ECT due to the brief pulse width and polyphasic cosine shape of MST pulses (see figure 2). Coronal views of the electric field relative to threshold for the seven stimulation modalities are shown in figure 3. The simulation results for maximum electric field (absolute and relative to neural activation threshold), superficiality, and brain volume with electric field above threshold and above half-maximum are summarized in figure 4.

3.1.1. Stimulation strength—Figure 4(a) shows the maximum electric field in the brain induced by ECT and MST. All ECT configurations induce similar maximum electric field strength in the brain, ranging from 2.14 V/cm to 2.51 V/cm, for RUL and FEAST, respectively. DCONE MST induces similar maximum electric field strength (2.23 V/cm) compared with ECT. CIRC MST produces the lowest electric field strength among all configurations.

As illustrated in figure 3 and figure 4(b), even though ECT and MST produce similar maximum electric field, the stimulation strengths of MST relative to the neural activation threshold is significantly lower than that of ECT due to the higher E_{th} for MST. The maximum ECT induced electric field strength ranges from 6.2 to 7.2 times threshold, for RUL and FEAST, respectively, whereas the values for MST are much lower, ranging from 1.2 to 2.3 times threshold, for CIRC and DCONE, respectively. If ECT is administered with a pulse width of 1 ms instead of 0.3 ms, the electric field strength relative to threshold would increase by 14%.

3.1.2. Stimulation focality—Figure 4(c) shows the maximum electric field as a function of depth in the brain. The MST electric field attenuates more rapidly in depth than the ECT electric field, reaching zero at the center of the brain. The maximum electric field strength is higher in the superficial gray matter than in the white matter for all modalities except for BL and FEAST ECT. Unlike BL and FEAST, the BF and RUL electric field discontinuity at the

gray matter–white matter interface is negligible since the electric field there is mostly tangential. Similarly, the MST electric field magnitude is continuous across the gray matter–white matter interface since the electric field is tangential anywhere in the sphere. Of all configurations, BL ECT produces the strongest electric field in depth relative to the surface of the brain.

Figure 4(d) shows the percentage of brain volume stimulated above threshold, Vol($E \geq E_{th}$), which is much higher with ECT than with MST (up to 100% for ECT, and up to 8.17% for MST). Of note, BL ECT produces suprathreshold electric field in 100% of the brain volume, and BF, RUL, and FEAST ECT produce suprathreshold electric field in over 90% of the brain volume. Figure 4(d) also shows the intrinsic focality assessed by the brain volume stimulated above the half-maximum electric field, Vol($E \geq E_{max}/2$). Among the seven stimulation modalities, DCONE MST has the best intrinsic focality, whereas BL ECT is the most nonfocal. The intrinsic focalities of BF and RUL ECT, and CIRC and CAP MST are similar. Notably, FEAST is not only the most focal among ECT configurations, but is also intrinsically more focal than two of the MST configurations (CIRC and CAP).

4. Discussion

4.1. ECT vs. MST induced electric field

Our simulation results indicate that MST provides less intense and more focal stimulation than ECT, as seen in figures 3 and 4. These results support the original motivation for the development of MST as a more targeted form of seizure induction, proposed as a means to reduce the side effects of ECT [9, 93]. In contrast, in ECT large portions of the brain (up to 100%) are stimulated at high intensities relative to neuronal threshold (up to 7.2 times threshold). MST is more confined to the superficial cortex than ECT [figure 3 and 4(c)], consistent with our *in vivo* induced voltage data [94]. Therefore, MST may reduce the cognitive side effects of convulsive therapy, as there is limited direct stimulation of medial–temporal brain structures, such as the hippocampus.

In present clinical ECT practice, a fixed pulse amplitude of 800 or 900 mA is delivered to all patients. Our results indicate that at this pulse amplitude the electric field in the brain exceeds the threshold for robust neural activation by more than 6 fold, much higher than necessary for seizure induction and possibly contributing to the adverse side effects of ECT. There is substantial evidence in the literature that pulse amplitudes lower than 800 mA can successfully trigger seizures, and can have therapeutic effect with potentially reduced side effects (for review see [11]). Furthermore, MST can elicit therapeutic seizures [95, 96] despite producing, according to our results, stimulation strength 3–6 times weaker and focality 10–60 times higher than conventional ECT with 800 mA, 0.3 ms pulses. Remarkably, BF, RUL, and FEAST ECT have similar intrinsic focality to CIRC and CAP MST, as shown in figure 4(d). This implies that by lowering the current amplitude, the stimulation focality of ECT with particular electrode configurations can be made similar to that of MST. As per (5), reducing the pulse width can also decrease the strength of stimulation by increasing E_{th}. Thus, ECT with lower than conventional pulse amplitude and/or pulse width may still be able to induce therapeutic seizures while reducing cognitive side effects. The utility of this approach awaits evaluation in clinical trials.

4.2. Comparison of ECT electrode and MST coil configurations

4.2.1. ECT—Among the ECT electrode configurations, BL directly activated the largest brain volume(100%) and was the least focal, having Vol($E \geq E_{max}/2$) of over 4 times those of BF, RUL, and FEAST. BL ECT also has the slowest electric field attenuation in depth, providing the strongest deep brain stimulation among electrode configurations. BF and RUL

ECT showed nearly identical electric field characteristics since the electrode separations for the two configurations are nearly equal. In a realistic head, both electrode separation and placement affect the induced electric field distribution (the limitations of the spherical head model are discussed further in section 4.3). The FEAST paradigm was proposed to achieve more focal seizure induction [8, 92]. We found that FEAST has the highest intrinsic focality [lowest Vol($E \geq E_{max}/2$)] among ECT configurations and is in fact more focal than CIRC and CAP MST. However, at current of 800 mA we found no substantial difference in directly activated brain volume, Vol($E \geq E_{th}$), between FEAST and BF and RUL ECT. Therefore, to utilize the superior intrinsic focality of the FEAST configuration, it should be used with lower current amplitudes. Lowering current amplitude would also improve the focality of the conventional ECT electrode placements, as discussed in the previous section.

Our results on ECT electric field strength (2.1–2.5 V/cm maximum) correspond well with published intracranial induced voltage data. Measurements in cadaver heads yield electric field strength estimates of 0.7–1.8 V/cm for BL electrode placement with 800 mA current [12, 13]. Measurements of a half-skull immersed in a head-shaped electrolytic tank with frontal–occipital electrodes give electric field ranging from 1.5 V/cm near the brain center to 2.5 V/cm near the brain–skull interface for 800 mA current [14]. These *ex vivo* electric field estimates match our ECT models within 10–20%. Our simulated values for the maximum ECT electric field strength fall in the middle of the range reported in previous theoretical and simulation studies (0.9–5 V/cm for 800 mA current) [14, 25-27].

4.2.2. MST—Among the MST coil configurations, DCONE induced the strongest and slightly deeperelectric field, consistent with the notion that coils with larger dimensions induce electric fields withslower attenuation in depth [97]. DCONE MST is also the most focal, having Vol($E \geq E_{max}/2$) more than 2 times less than those of CIRC and CAP MST. CIRC MST induced the weakest, most superficial electric field and the smallest activated brain volume (1.6%). CAP MST activated the largest brain volume (8.2%) and had the worst intrinsic focality among coil configurations. These coil configurations differ in their seizure inducing capabilities: DCONE is most efficient, CAP—second most efficient, and CIRC—least efficient [95, 96], correlating with the maximum induced electric field strength relative to threshold shown in figure 4(b). However, the impact on clinical outcomes of these differences is not clear. In fact, we found no difference in efficacy or side effects between DCONE and CAP MST coils [95, 96], potentially due to the fact that they are both very focal.

A key clinical question is whether the reduced stimulation strength and increased focality of MST preferentially reduces side effects while preserving efficacy. In the first controlled trial of MST, the treatments were shown to have significant antidepressant benefit and an excellent safety profile in a group of severely depressed patients referred for ECT [96]. MST had less neurocognitive side effects compared to published reports of ECT. The observed remission rate with MST was lower than that reported with the most robust forms of ECT, such as standard pulse width (1 ms) BL ECT. However, MST had higher antidepressant efficacy than rTMS [98], which is approved for the treatment of depression by the U.S. Food and Drug Administration. Finally, it should be noted that in that study, the MST stimulus was limited in duration due to device output limitations. Thus, the study might have underestimated the potential antidepressant efficacy of MST.

The MST electric field strengths in our study (1.1–2.2 V/cm maximum) are in the midrange of previous simulation results which report values of 0.16–5 V/cm for figure-8 and circular coils which are similar to the MST coils presented in this work in terms of product of coil current and number of turns of approximately 80 kA-turn [25, 26, 30-35, 99]. Finally, our

simulated DCONE MST electric field matches saline phantom measurements of the actual coil within 15% (see Supplementary Material).

4.3. Limitations and future work

4.3.1. Head mode—The spherical head model presented in this study has limitations. In reality, tissue layers have complex geometry, non-uniform thickness, and heterogeneous and anisotropic conductivity, and the skull has orifices such as the eye sockets and the auditory canals, representing potential low-impedance paths for electrical current. There is evidence that including realistic cortical folding in the model can increase the simulated maximum electric field strength by 50–70% compared to a spherical model [36, 100]. Thus, the spherical model may be underestimating the strength of neural stimulation for both electric and magnetic stimulation [36, 100-105]. In addition, lack of representation for subcortical structures, such as ventricles, obscures their contribution to the induced electric field distribution. As with cortical folding, the presence of ventricles filled with high-conductivity cerebrospinal fluid will likely increase the deep-brain electric field strength in the surrounding brain tissue. Since the ECT electric field decays slower in depth than the MST field [figure 4(c)], the presence of ventricles will likely amplify the stimulation strength in depth preferentially for ECT (especially for BL ECT). Therefore, the stimulation of deep-brain structures such as the hippocampus could be even stronger with ECT relative to MST than predicted by our spherical model. Taken together, the effects of cortical folding and subcortical ventricles both amplify our argument that the ECT current amplitude used in clinical practice may be much higher than necessary for seizure induction. Future work could use more anatomically accurate head models that also include tissue anisotropy and could analyze the electric field in specific brain regions thought to be associated with therapeutic benefits (e.g., medial prefrontal cortex, thalamus) or side effects (e.g., hippocampus, insula), as we have demonstrated with preliminary ECT modeling results [29].

We reported data for only the adult female head spherical model. We have previously reported preliminary data for men and women [38] which showed that, within the assumptions of the spherical model, the results for the two models are quantitatively and qualitatively similar. Therefore, in this paper we focused on one of the sexes. A large percentage of ECT patients are elderly. While head diameter and skull and scalp thicknesses are not expected to change during adulthood, elderly patients are likely to experience cerebral atrophy. The effect of decrease in brain volume on the electric field was explored in our anatomical variability study [38].

4.3.2. Neural activation threshold—We acknowledge that it is a substantial simplification to use a single electric field threshold for neural activation throughout the brain. The electric field threshold and neural time constant values used in section 2.2.1 to estimate the modality-specific thresholds were derived in the literature from empirically determined motor thresholds coupled with spherical computational models or phantom measurements of the electric field [76-79]. Thus, the cited electric field thresholds are subject to accuracy limitations similar to those of our spherical model. Furthermore, data linking neural response threshold and transcranially induced electric field strength have been published only for the motor cortex. As more accurate threshold data for motor cortex and other brain regions become available, it could be integrated in our model. For example, the thresholds for non-motor brain regions could be derived from data on after discharge and electroencephalographic evoked responses (see, e.g., [106, 107]).

Another limitation is that we use neural activation thresholds that are independent of the electric field direction, whereas the electric field direction relative to the stimulated neural

populations is known to affect the neural activation threshold. For example, the TMS motor threshold varies as a function of the induced current direction up to 35% [90, 108, 109]. Cathodal and anodal transcranial electrical stimulation, associated with opposite current flow, preferentially activate different neural elements [110-113]; nevertheless, the motor thresholds are similar for the two polarities [111, 114-116]. Variation in the electric field threshold would inverse-proportionally scale our stimulation strength estimate and would nonlinearly affect the directly activated brain volume. For example, a 35% increase in the electric field threshold would reduce the directly activated brain volume by approximately 25% for 0.3 ms pulse width RUL ECT. Besides direction, the spatial gradient of the electric field may also affect the threshold, especially for long, relatively straight white matter fibers, as discussed in section 2.2. Indeed, because of the different spatial characteristics of the electric field, transcranial electric and magnetic stimulation applied at threshold strength are known to affect different neuronal populations [108, 117]. Nevertheless, as discussed in section 2.2.1, the TMS electric field thresholds are comparable to those estimated for transcranial electrical stimulation with similar effective pulse width. Furthermore, compared to near-threshold transcranial electric and magnetic stimulation, MST and especially ECT stimulate wide regions of the brain which could contribute to partial averaging out of the effects of threshold variability among neural populations and electric field directions.

Finally, the membrane time constant of white matter fibers is not necessarily the same as that for gray matter, although the distributions of membrane time constants obtained from gray matter and white matter stimulation overlap considerably [118]. Indeed, the membrane time constant used in our study (τ_m = 150 μs) falls in the range of values estimated from clinical deep brain stimulation of white matter fibers associated with the thalamus (τ_m = 48–866 μs) [119-121], globus pallidus internus (τ_m = 53–1440 μs) [119, 122, 123], and subthalamic nucleus (τ_m = 72–173 μs) [124, 125]. Thus, our estimated neural membrane depolarization factors, $\max(|(w * h)(t)|)$ in table 2, are likely to be representative of white matter structures as well. Furthermore, besides the elicitation of action potentials in axons, which is thought to be the dominant mechanism of extracellular neural stimulation [85, 126], the induced electric field may have additional polarization effects on the soma and dendrites which have larger membrane time constants (∼ 10 ms) than axons [85, 110]. Therefore, dendrite and soma polarization may influence the behavior of neurons and neural circuits, especially in ECT paradigms with long pulse width (∼ 1 ms) and high electric field strength [11, 110, 127]. However, such putative second-order mechanisms have not been explored in detail, and, therefore, cannot be prudently integrated in our model.

At present it is challenging to incorporate detailed threshold characterization within a whole-head electric field model due to the diversity of neural populations and the lack of data on all relevant neural parameters [36, 110]. Nevertheless, despite the limitations of our model, our results suggest that ECT electric fields exceed the neural activation threshold by over 500%; therefore, some uncertainty in the threshold value is unlikely to change our qualitative conclusions.

4.3.3. Seizure therapy mechanisms—Finally, the simulations address only the electric field and not the seizure itself, the topography of which is also thought to be a major contributor to clinical outcome. Nevertheless, the induced electric field distribution relative to neural activation threshold indicates potential sites of seizure initiation. Seizure initiation and propagation likely depend on both the direct neural stimulation and the intrinsic excitability and connectivity of neural circuits. In this study, we have shown that all ECT configurations induce suprathreshold electric fields in nearly the whole brain, although the degree to which the threshold is exceeded in various brain regions differs widely among electrode configurations. While several studies showed that virtually all neurons in the brain are involved in generalized tonic-clonic seizures [128-130], other suggest that selective

frontal, parietal, and temporal networks are preferentially involved in generalized seizures [131-133]. Correlation of electric field maps with neuroimaging data on the initiation and spread of seizures could provide further insight into the mechanisms of convulsive therapy.

5. Conclusions

This is the first study to systematically compare the electric field induced in the brain by existing forms of ECT and MST. The simulated electric field strengths are consistent with published *in vivo*, *ex vivo*, theoretical, and simulation results, as well as with our MST phantom measurements. We also introduced a method of incorporating a modality-specific neural activation threshold in the electric field models that can inform dosage requirements for ECT and MST.

Contrasting ECT and MST configurations that differ markedly in efficacy, side effects, and seizure induction efficiency could advance our understanding of the principles linking treatment parameters and therapeutic outcome and could provide a means of testing hypotheses of the mechanisms of convulsive therapies. We found notable differences between ECT and MST: the electric field relative to threshold for MST is 3–6 times weaker, more superficial, and 10–60 times more focal compared with conventional ECT with 800 mA, 0.3 ms pulses. Our results suggest that at a pulse amplitude of 800 mA, the electric field induced by ECT exceeds the threshold for robust neural activation by more than 6 times, much higher than necessary for seizure induction. Reducing the ECT pulse amplitude would bring the electric field strength down closer to threshold and would increase the focality of ECT. Given that more focal stimulation with weaker electric field in MST already shows significantly fewer side effects than ECT, the impact of ECT pulse amplitude reduction on adverse side effects bears further examination.

Supplementary Material

Refer to Web version on PubMed Central for supplementary material.

Acknowledgments

This work was supported by National Institutes of Health grants NCRR 5TL1RR024158-03 and MH60884.

Disclosure: ZDD, SHL, and AVP are inventors on Columbia University patent applications on TMS and MST technology. AVP has received equipment support from Magstim and ANS/St. Jude Medical. SHL has received equipment support from Magstim and MagVenture, and research grants from ANS/St. Jude Medical, Neuronetics, Cyberonics, Brainsway, NIH, AFAR, NARSAD, Stanley Medical Research Foundation, DARPA, and NYSTAR.

References

1. Sackeim HA, Prudic J, Fuller R, Keilp J, Lavori PW, Olfson M. The cognitive effects ofelectroconvulsive therapy in community settings. Neuropsychopharmacology. 2007; 32:244–54. [PubMed: 16936712]
2. Nuttall GA, Bowersox MR, Douglass SB, McDonald J, Rasmussen LJ, Decker PA, Oliver WC Jr, Rasmussen KG. Morbidity and mortality in the use of electroconvulsive therapy. J ECT. 2004; 20:237–41. [PubMed: 15591857]
3. Sackeim HA, Prudic J, Devanand DP, Nobler MS, Lisanby SH, Peyser S, Fitzsimons L, Moody BJ, Clark J. A prospective, randomized, double-blind comparison of bilateral and right unilateral electroconvulsive therapy at different stimulus intensities. Arch Gen Psychiatry. 2000; 57:425–34. [PubMed: 10807482]
4. Squire LR, Zouzounis JA. ECT and memory: brief pulse versus sine wave. Am J Psychiatry. 1986; 143:596–601. [PubMed: 3963246]

5. Weiner RD, Rogers HJ, Davidson JR, Squire LR. Effects of stimulus parameters on cognitive side effects. Ann N Y Acad Sci. 1986; 462:315–25. [PubMed: 3458412]
6. Sackeim HA, Prudic J, Nobler MS, Fitzsimons L, Lisanby SH, Payne N, Berman RM, Brakemeier EL, Perera T, Devanand DP. Effects of pulse width and electrode placement on the efficacy and cognitive effects of electroconvulsive therapy. Brain Stimul. 2008; 1:71–83. [PubMed: 19756236]
7. Abrams, R. Electroconvulsive Therapy. New York: Oxford Unversity Press; 2002.
8. Sackeim HA. Convulsant and anticonvulsant properties of electroconvulsive therapy: towards a focal form of brain stimulation. Clin Neurosci Res. 2004; 4:39–57.
9. Lisanby SH, Luber B, Schlaepfer TE, Sackeim HA. Safety and feasibility of magnetic seizure therapy (MST) in major depression: randomized within-subject comparison with electroconvulsive therapy. Neuropsychopharmacology. 2003; 28:1852–65. [PubMed: 12865903]
10. Kellner CH, Tobias KG, Wiegand J. Electrode placement in electroconvulsive therapy (ECT): a review of the literature. J ECT. 2010; 26:175–80. [PubMed: 20562639]
11. Peterchev AV, Rosa MA, Deng ZD, Prudic J, Lisanby SH. ECT stimulus parameters: rethinking dosage. J ECT. 2010; 26:159–74. [PubMed: 20805726]
12. Smitt JW, Wegener CF. On electric convulsive therapy with particular regard to a pariental application of electrodes controlled by intracerebral voltage measurements. Acta Psychiatr Neurol. 1944; 19:529–49.
13. Lorimer FM, Segal MM, Stein SN. Path of current distribution in brain during electro-convulsive therapy. Electroencephalogr Clin Neurophysiol. 1949; 1:343–8. [PubMed: 18135426]
14. Rush S, Driscoll DA. Current distribution in the brain from surface electrodes. Anesth Analg. 1968; 47:717–23. [PubMed: 4972743]
15. Wagner TA, Gangitano M, Romero R, Theoret H, Kobayashi M, Anschel D, Ives J, Cuffin N, Schomer D, Pascual-Leone A. Intracranial measurement of current densities induced by transcranial magnetic stimulation in the human brain. Neurosci Lett. 2004; 354:91–4. [PubMed: 14698446]
16. Hayes KJ. The current path in electric convulsive shock. Arch Neurol Psychiatry. 1950; 63:102–9.
17. Lisanby SH, Moscrip TD, Morales O, Luber B, Schroeder C, Sackeim HA. Neurophysiological characterization of magnetic seizure therapy (MST) in non-human primates. Clin Neuophysiol Suppl. 2003; 56:81–99.
18. Weissman JD, Epstein CM, Davey KR. Magnetic brain stimulation and brain size: relevance to animal studies. Electroencephalogr Clin Neurophysiol. 1992; 85:215–9. [PubMed: 1376680]
19. Deng ZD, Peterchev AV, Lisanby SH. Focality of neural stimulation with magnetic seizure therapy (MST) and electroconvulsive therapy (ECT) in humans and non-human primates. 64th Ann Conv Soc Biol Psychiatry. 2009
20. Weaver L, Williams R, Rush S. Current density in bilateral and unilateral ECT. Biol Psychiatry. 1976; 11:303–12. [PubMed: 938698]
21. Saypol JM, Roth BJ, Cohen LG, Hallett M. A theoretical comparison of electric and magnetic stimulation of the brain. Ann Biomed Eng. 1991; 19:317–28. [PubMed: 1928873]
22. Stecker MM. Transcranial electric stimulation of motor pathways: a theoretical analysis. Comput Biol Med. 2005; 35:133–55. [PubMed: 15567183]
23. Zyss T, Krawczyk A, Drzymala P, Starzynski J. ECT versus transcranial magnetic stimulation (TMS): preliminary data of computer modeling. Psychiatr Pol. 1999; 33:909–23. [PubMed: 10776027]
24. Sekino M, Ueno S. Comparison of current distributions in electroconvulsive therapy and transcranial magnetic stimulation. J Appl Phys. 2002; 91:8730–2.
25. Nadeem M, Thorlin T, Gandhi OP, Persson MA. Computation of electric and magnetic stimulation in human head using the 3-D impedance method. IEEE Trans Biomed Eng. 2003; 50:900–7. [PubMed: 12848358]
26. Sekino M, Ueno S. FEM-based determination of optimum current distribution in transcranial magnetic stimulation as an alternative to electroconvulsive therapy. IEEE Trans Mag. 2004; 40:2167–9.

27. Szmurło R, Sawicki B, Starzyński J, Wincenciak S. A comparison of two models of electrodes for ECT simulations. IEEE Trans Mag. 2006; 42:1395–8.
28. Holdefer RN, Sadleir RJ, Russell MJ. Predicted current densities in the brain during transcranial electrical stimulation. Clin Neurophysiol. 2006; 117:1388–97. [PubMed: 16644273]
29. Lee WH, Deng ZD, Kim TS, Laine AF, Lisanby SH, Peterchev AV. Regional electric field induced by electroconvulsive therapy: a finite element simulation study. Conf Proc IEEE Eng Med Biol Soc. 2010:2045–8. [PubMed: 21096148]
30. Cerri G, De Leo R, Moglie F, Schiavoni A. An accurate 3-D model for magnetic stimulation of the brain cortex. J Med Eng Technol. 1995; 19:7–16. [PubMed: 7562982]
31. Chen M, Mogul DJ. A structurally detailed finite element human head model for simulation of transcranial magnetic stimulation. J Neurosci Methods. 2009; 179:111–20. [PubMed: 19428517]
32. Toschi N, Welt T, Guerrisi M, Keck ME. A reconstruction of the conductive phenomena elicited by transcranial magnetic stimulation in heterogeneous brain tissue. Phys Med. 2008; 24:80–6. [PubMed: 18296093]
33. Toschi N, Welt T, Guerrisi M, Keck ME. Transcranial magnetic stimulation in heterogeneous brain tissue: clinical impact on focality, reproducibility and true sham stimulation. J Psychiatr Res. 2009; 43:255–64. [PubMed: 18514227]
34. Wagner TA, Zahn M, Grodzinsky AJ, Pascual-Leone A. Three-dimensional head model simulation of transcranial magnetic stimulation. IEEE Trans Biomed Eng. 2004; 51:1586–98. [PubMed: 15376507]
35. Wagner TA, Fregni F, Eden U, Ramos-Estebanez C, Grodzinsky AJ, Zahn M, Pascual-Leone A. Transcranial magnetic stimulation and stroke: a computer-based human model study. NeuroImage. 2006; 30:857–70. [PubMed: 16473528]
36. Thielscher A, Opitz A, Windhoff M. Impact of the gyral geometry on the electric field induced by transcranial magnetic stimulation. NeuroImage. 2010; 54:234–43. [PubMed: 20682353]
37. Geddes LA. Optimal stimulus duration for extracranial cortical stimulation. Neurosurgery. 1987; 20:94–9. [PubMed: 3808283]
38. Deng ZD, Lisanby SH, Peterchev AV. Effect of anatomical variability on neural stimulation strength and focality in electroconvulsive therapy (ECT) and magnetic seizure therapy (MST). Conf Proc IEEE Eng Med Biol Soc. 2009:682–8. [PubMed: 19964484]
39. Rudorfer, MV.; Henry, ME.; Sackeim, HA. Psychiatry. Tasman, A., et al., editors. Chichester: John Wiley & Sons Ltd; 2003. p. 1865-901.
40. Manjunath KY. Estimation of cranial volume in dissecting room cadavers. J Anat Soc India. 2002; 51:168–72.
41. Örmeei AR, Gürbüz H, Ayata A, Çetin H. Adult head circumferences and centiles. J Turgut Özal Med Cent. 1997; 4:261–4.
42. Hori H, Moretti G, Rebora A, Crovato F. The thickness of human scalp: normal and bald. J Invest Dermatol. 1972; 58:396–9. [PubMed: 5030661]
43. Lupin AJ, Gardiner RJ. Scalp thickness in the temporal region: its relevance to the development of cochlear implants. Cochlear Implants Int. 2001; 2:30–8. [PubMed: 18792002]
44. Li H, Ruan J, Xie Z, Wang H, Liu W. Investigation of the critical geometric characteristics of living human skulls utilising medical image analysis techniques. Int J Veh Saf. 2007; 2:345–67.
45. Baumann SB, Wozny DR, Kelly SK, Meno FM. The electrical conductivity of human cerebrospinal fluid at body temperature. IEEE Trans Biomed Eng. 1997; 44:220–3. [PubMed: 9216137]
46. Gabriel S, Lau RW, Gabriel C. The dielectric properties of biological tissues: II. Measurements in the frequency range 10 Hz to 20 GHz. Phys Med Biol. 1996; 41:2251–69. [PubMed: 8938025]
47. Geddes LA, Baker LE. The specific resistance of biological material--a compendium of data for the biomedical engineer and physiologist. Med Biol Eng Comput. 1967; 5:271–93.
48. Wolters CH, Anwander A, Tricoche X, Weinstein D, Koch MA, MacLeod RS. Influence of tissue conductivity anisotropy on EEG/MEG field and return current computation in a realistic head model: a simulation and visualization study using high-resolution finite element modeling. NeuroImage. 2006; 30:813–26. [PubMed: 16364662]

49. Gabriel S, Lau RW, Gabriel C. The dielectric properties of biological tissues: III. Parametric models for the dielectric spectrum of tissues. Phys Med Biol. 1996; 41:2271–93. [PubMed: 8938026]
50. Bossetti CA, Birdno MJ, Grill WM. Analysis of the quasi-static approximation for calculating potentials generated by neural stimulation. J Neural Eng. 2008; 5:44–53. [PubMed: 18310810]
51. Homma S, Musha T, Nakajima Y, Okamoto Y, Blom S, Flink R, Hagbarth KE. Conductivity ratios of the scalp-skull-brain head model in estimating equivalent dipole sources in human brain. Neurosci Res Commun. 1995; 22:51–5.
52. Rush S, Driscoll DA. EEG electrode sensitivity—an application of reciprocity. IEEE Trans Biomed Eng. 1969; 16:15–22. [PubMed: 5775600]
53. Gonçalve SI, de Munck JC, Verbunt JPA, Bijma F, Heethaar RM, da Silva FHL. In vivo measurement of the brain and skull resistivities using an EIT-based method and realistic models for the head. IEEE Trans Biomed Eng. 2003; 50:754–67. [PubMed: 12814242]
54. Lai Y, van Drongelen W, Ding L, Hecox HE, Towle VL, Frim DM, He B. Estimation of in vivo human brain-to-skull conductivity ratio by means of cortical potential imaging. Int J Bioelectromagn. 2005; 7:311–2.
55. Zhang Y, van Drongelen W, He B. Estimation of in vivo brain-to-skull conductivity ratio in human. Appl Phys Lett. 2006; 89:223903–2239033. [PubMed: 17492058]
56. Oostendorp TF, Delbeke J, Stegeman DF. The conductivity of the human skull: results of in vivo and in vitro measurements. IEEE Trans Biomed Eng. 2000; 47:1487–91. [PubMed: 11077742]
57. Sadleir RJ, Argibay A. Modeling skull electrical properties. Ann Biomed Eng. 2007; 35:1699–712. [PubMed: 17629793]
58. APA. The Practice of Electroconvulsive Therapy: Recommendations for Treatment, and Privileging: A Task Force Report of the American Psychiatric Association. Washington, D.C: American Psychiatric Association; 2001.
59. Plonsey R, Heppner D. Considerations of quasi-stationarity in electrophysiological systems. Bull Math Biol. 1967; 29:657–64.
60. Roth BJ, Cohen LG, Hallett M, Friauf W, Basser PJ. A theoretical calculation of the electric field induced by magnetic stimulation of a peripheral nerve. Muscle Nerve. 1990; 13:734–41. [PubMed: 2385260]
61. Schwan HP, Kay CF. Capacitive properties of body tissues. Circul Res. 1957; 5:439–43.
62. Webb JP, Forghani B. T-Ω method using hierarchal edge elements. IEE Proc Sci Meas Tech. 1995; 142:133–41.
63. Infolytica Corp. ElecNet/MagNet: 2D/3D electromagnetic field simulation software documentation. Montréal, Québec, Canada: 2009.
64. Rattay F. Analysis of models for external stimulation of axons. IEEE Trans Biomed Eng. 1986; 33:974–7. [PubMed: 3770787]
65. Warman EN, Grill WM, Durand DM. Modeling the effects of electric fields on nerve fibers: determination of excitation thresholds. IEEE Trans Biomed Eng. 1992; 39:1244–54. [PubMed: 1487287]
66. Maccabee PJ, Amassian VE, Eberle LP, Cracco RQ. Magnetic coil stimulation of straight and bent amphibian and mammalian peripheral nerve in vitro: locus of excitation. J Physiol (Lond). 1993; 460:201–19. [PubMed: 8487192]
67. Abdeen MA, Stuchly MA. Modeling of magnetic field stimulation of bent neurons. IEEE Trans Biomed Eng. 1994; 41:1092–5. [PubMed: 8001998]
68. Reilly JP. Peripheral nerve stimulation by induced electric currents: exposure to time-varying magnetic fields. Med Biol Eng Comput. 1989; 27:101–10. [PubMed: 2689806]
69. Hyodo A, Ueno S. Nerve excitation model for localized magnetic stimulation of finite neuronal structures. IEEE Trans Mag. 1996; 32:5112–4.
70. Ruohonen J, Ilmoniemi RJ. Modelling of the stimulating field generation in TMS. Electroencephalogr Clin Neurophysiol Suppl. 1999; 51:30–40. [PubMed: 10590933]
71. Tranchina D, Nicholson C. A model for the polarization of neurons by extrinsically applied electric fields. Biophys J. 1986; 50:1139–56. [PubMed: 3801574]

72. Ruohonen, J.; Ilmoniemi, RJ. Handbook of Transcranial Magnetic Stimulation. Pascual-Leone, A., et al., editors. London: Arnold; 2002. p. 18-30.
73. Morioka T, Yamamoto T, Mizushima A, Tombimatsu S, Shigeto H, Hasuo K, Nishio S, Fujii K, Fukui M. Comparison of magnetoencephalography, functional MRI, and motor evoked potentials in the localization of the sensory-motor cortex. Neurol Res. 1995; 17:361–7. [PubMed: 8584127]
74. Krings T, Buchbinder BR, Butler WE, Chiappa KH, Jiang HJ, Rosen BR, Cosgrove GR. Stereotactic transcranial magnetic stimulation: correlation with direct electrical cortical stimulation. Neurosurgery. 1997; 41:1319–25. [PubMed: 9402583]
75. Wassermann EM, Wang B, Zeffiro TA, Sadato N, Pascual-Leone A, Toro C, Hallett M. Locating the motor cortex on the MRI with transcranial magnetic stimulation and PET. NeuroImage. 1996; 3:1–9. [PubMed: 9345470]
76. Rudiak D, Marg E. Finding the depth of magnetic brain stimulation: a re-evaluation. Electroencephalogr Clin Neurophysiol Suppl. 1994; 93:358–71.
77. Epstein CM, Schwartzberg DG, Davey KR, Sudderth DB. Localizing the site of magnetic brain stimulation in humans. Neurology. 1990; 40:666–70. [PubMed: 2320243]
78. Thielscher A, Kammer T. Linking physics and physiology in TMS: a sphere field model to determine the cortical stimulation site in TMS. NeuroImage. 2002; 17:1117–30. [PubMed: 12414254]
79. Komssi S, Savolainen P, Heiskala J, Kahkonen S. Excitation threshold of the motor cortex estimated with transcranial magnetic stimulation electroencephalography. Neuroreport. 2007; 18:13–6. [PubMed: 17259853]
80. Calancie B, Harris W, Broton JG, Alexeeva N, Green BA. “Threshold-level” multipulse transcranial electrical stimulation of motor cortex for intraoperative monitoring of spinal motor tracts: description of method and comparison to somatosensory evoked potential monitoring. J Neurosurg. 1998; 88:457–70. [PubMed: 9488299]
81. Pitcher JB, Ogston KM, Miles TS. Age and sex differences in human motor cortex input-output characteristics. J Physiol (Lond). 2003; 546:605–13. [PubMed: 12527746]
82. Barker AT, Garnham CW, Freeston IL. Magnetic nerve stimulation: the effect of waveform on efficiency, determination of neural membrane time constants and the measurement of stimulator output. Electroencephalogr Clin Neurophysiol Suppl. 1991; 43:227–37. [PubMed: 1773760]
83. Plonsey R, Barr RC. Electric field stimulation of excitable tissue. IEEE Eng Med Biol Mag. 1998; 17:130–7. [PubMed: 9770615]
84. Jezernik S, Sinkjaer T, Morari M. Charge and energy minimization in electrical/magnetic stimulation of nervous tissue. J Neural Eng. 2010; 7:046004. [PubMed: 20551509]
85. Nowak LG, Bullier J. Axons, but not cell bodies, are activated by electrical stimulation in cortical gray matter I. Evidence from chronaxie measurements. Exp Brain Res. 1998; 118:477–88. [PubMed: 9504843]
86. Peterchev AV, Jalinous R, Lisanby SH. A transcranial magnetic stimulator inducing near-rectangular pulses with controllable pulse width (cTMS). IEEE Trans Biomed Eng. 2008; 55:257–66. [PubMed: 18232369]
87. Radman T, Ramos RL, Brumberg JC, Bikson M. Role of cortical cell type and morphology in subthreshold and suprathreshold uniform electric field stimulation in vitro. Brain Stimul. 2009; 2:215–28. [PubMed: 20161507]
88. Kähkönen S, Wilenius J, Komssi S, Ilmoniemi RJ. Distinct differences in cortical reactivity of motor and prefrontal cortices to magnetic stimulation. Clin Neurophysiol. 2004; 115:583–8. [PubMed: 15036054]
89. Kähkönen S, Komssi S, Wilenius J, Ilmoniemi RJ. Prefrontal transcranial magnetic stimulation produces intensity-dependent EEG responses in humans. NeuroImage. 2005; 24:955–60. [PubMed: 15670672]
90. Balslev D, Braet W, McAllister C, Miall RC. Inter-individual variability in optimal current direction for transcranial magnetic stimulation of the motor cortex. J Neurosci Methods. 2007; 162:309–13. [PubMed: 17353054]

91. Sackeim HA, Long J, Luber B, Moeller JR, Prohovnik I, Devanand DP, Nobler MS. Physical properties and quantification of the ECT stimulus: I. Basic principles. Convuls Ther. 1994; 10:93–123. [PubMed: 8069647]
92. Spellman T, Peterchev AV, Lisanby SH. Focal electrically administered seizure therapy: a novel form of ECT illustrates the roles of current directionality, polarity, and electrode configuration in seziure induction. Neuropsychopharmacology. 2009; 34:2002–10. [PubMed: 19225453]
93. Sackeim HA. Magnetic stimulation therapy and ECT. Convuls Ther. 1994; 10:255–8.
94. Lisanby, SH.; Moscrip, TD.; Morales, O.; Luber, B.; Schroeder, C.; Sackeim, HA. Transcranial Magnetic Stimulation and Transcranial Direct Current Stimulation (Supplements to Clinical Neurophysiology). Paulus, W., et al., editors. Elsevier Science; 2003.
95. Lisanby SH, Husain MM, Morales OG, Thornton WL, White PF, Payne N, Rush AJ, Sackeim HA. Controlled clinical trial of the antidepressant efficacy of magnetic seizure therapy in the treatment of major depression. Am Coll Neuropsychopharmacol Ann Mtg. 2003:166.
96. Lisanby SH, McClintock SM, Luber B, Morales OG, Thornton WLF, White PF, Stool L, Rowny S, Nobler MS, Rush AJ, Husain M. Safety and efficacy of magnetic seizure therapy (MST) in the treatment of major depression: Randomized controlled trial of two MST coils. In review. 2010
97. Deng ZD, Peterchev AV, Lisanby SH. Coil design considerations for deep-brain transcranial magnetic stimulation (dTMS). Conf Proc IEEE Eng Med Biol Soc. 2008:5675–9. [PubMed: 19164005]
98. O'Reardon JP, Solvason HB, Janicak PG, Sampson S, Isenberg KE, Nahas Z, McDonald WM, Avery D, Fitzgerald PB, Loo C, Demitrack MA, George MS, Sackeim HA. Efficacy and safety of transcranial magnetic stimulation in the acute treatment of major depression: a multisite randomized controlled trial. Biol Psychiatry. 2007; 62:1208–16. [PubMed: 17573044]
99. Roth BJ, Saypol JM, Hallett M, Cohen LG. A theoretical calculation of the electric field induced in the cortex during magnetic stimulation. Electroencephalogr Clin Neurophysiol. 1991; 81:47–56. [PubMed: 1705219]
100. Miranda PC, Hallett M, Basser PJ. The electric field induced in the brain by magnetic stimulation: a 3-D finite-element analysis of the effect of tissue heterogeneity and anisotropy. IEEE Trans Biomed Eng. 2003; 50:1074–85. [PubMed: 12943275]
101. Miranda PC, Correia L, Salvador R, Basser PJ. Tissue heterogeneity as a mechanism for localized neural stimulation by applied electric fields. Phys Med Biol. 2007; 52:5603–17. [PubMed: 17804884]
102. Silva S, Basser PJ, Miranda PC. Elucidating the mechanisms and loci of neuronal excitation by transcranial magnetic stimulation using a finite element model of a cortical sulcus. Clin Neurophysiol. 2008; 119:2405–13. [PubMed: 18783986]
103. Datta A, Bikson M, Fregni F. Transcranial direct current stimulation in patients with skull defects and skull plates: High-resolution computational FEM study of factors altering cortical current flow. NeuroImage. 2010; 52:1268–78. [PubMed: 20435146]
104. Salvador R, Mekonnen A, Ruffini G, Miranda PC. Modeling the electric field induced in a high resolution realistic head model during transcranial current stimulation. Conf Proc IEEE Eng Med Biol Soc. 2010:2073–6. [PubMed: 21095946]
105. Manola L, Roelofsen BH, Holsheimer J, Marani E, Geelen J. Modelling motor cortex stimulation for chronic pain control: electrical potential field, activating functions and responses of simple nerve fibre models. Med Biol Eng Comput. 2005; 43:335–43. [PubMed: 16035221]
106. Lesser RP, Lüders H, Klem G, Dinner DS, Morris HH, Hahn J. Cortical afterdischarge and functional response threshold: results of extraoperative testing. Epilepsia. 1984; 25:615–21. [PubMed: 6479112]
107. Kähkönen S, Komssi S, Wilenius J, Ilmoniemi RJ. Prefrontal TMS produces smaller EEG responses than motor-cortex TMS: implications for rTMS treatment in depression. Psychopharmacology. 2005; 181:16–20. [PubMed: 15719214]
108. Di Lazzaro V, Oliviero A, Mazzone P, Insola A, Pilato F, Saturno E, Accurso A, Tonali P, Rothwell JC. Comparison of descending volleys evoked by monophasic and biphasic magnetic stimulation of the motor cortex in conscious humans. Exp Brain Res. 2001; 141:121–7. [PubMed: 11685416]

109. Kammer T, Beck S, Thielscher A, Laubis-Herrmann U, Topka H. Motor thresholds in humans: a transcranial magnetic stimulation study comparing different pulse waveforms, current directions and stimulator types. Clin Neurophysiol. 2001; 112:250–8. [PubMed: 11165526]
110. Manola L, Holsheimer J, Veltink P, Buitenweg JR. Anodal vs cathodal stimulation of motor cortex: a modeling study. Clin Neurophysiol. 2007; 118:464–74. [PubMed: 17150409]
111. Hern JEC, Landgren S, Phillips CG, Porter R. Selective excitation of corticofugal neurones by surface-anodal stimulation of the baboon's motor cortex. J Physiol. 1962; 161:73–90. [PubMed: 13906736]
112. Rothwell JC, Thompson PD, Day BL, Dick JPR, Kachi T, Cowan JMA, Marsden CD. Motor cortex stimulation in intact man. 1. General characteristics of EMG responses in different muscles. Brain. 1987; 110:1173–90. [PubMed: 3676697]
113. Day BL, Rothwell JC, Thompson PD, Dick JP, Cowan JM, Berardelli A, Marsden CD. Motor cortex stimulation in intact man. 2. Multiple descending volleys. Brain. 1987; 110:1191–209. [PubMed: 3676698]
114. Burke D, Hicks RG, Stephen JP. Corticospinal volleys evoked by anodal and cathodal stimulation of the human motor cortex. J Physiol. 1990; 425:283–99. [PubMed: 2213580]
115. Hanajima R, Ashby P, Lang AE, Lozano AM. Effects of acute stimulation through contacts placed on the motor cortex for chronic stimulation. Clin Neurophysiol. 2002; 113:635–41. [PubMed: 11976043]
116. Libet B, Alberts WW, Wright EW, DeLattre LD, Levin G, Feinstein B. Production of threshold levels of conscious sensation by electrical stimulation of human somatosensory cortex. J Neurophysiol. 1964; 27:546–78. [PubMed: 14194958]
117. Rothwell JC. Physiological studies of electric and magnetic stimulation of the human brain. Electroencephalogr Clin Neurophysiol Suppl. 1991; 43:29–35. [PubMed: 1773767]
118. Kiss ZHT, Anderson T, Hansen T, Kirstein D, Suchowersky O, Hu B. Neural substrates of microstimulation-evoked tingling: a chronaxie study in human somatosensory thalamus. Eur J Neurosci. 2003; 18:728–32. [PubMed: 12911770]
119. Holsheimer J, Dijkstra EA, Demeulemeester H, Nuttin B. Chronaxie calculated from current-duration and voltage-duration data. J Neurosci Methods. 2000; 97:45–50. [PubMed: 10771074]
120. Strafella A, Ashby P, Munz M, Dostrovsky JO, Lozano AM, Lang AE. Inhibition of voluntary activity by thalamic stimulation in humans: relevance for the control of tremor. Mov Disord. 1997; 12:727–37. [PubMed: 9380056]
121. McIntyre CC, Grill WM, Sherman DL, Thakor NV. Cellular effects of deep brain stimulation: model-based analysis of activation and inhibition. J Neurophysiol. 2004; 91:1457–69. [PubMed: 14668299]
122. Ashby P, Strafella A, Dostrovsky JO, Lozano A, Lang AE. Immediate motor effects of stimulation through electrodes implanted in the human globus pallidus. Stereotact Funct Neurosurg. 1998; 70:1–18. [PubMed: 9691237]
123. Wu YR, Levy R, Ashby P, Tasker RR, Dostrovsky JO. Does stimulation of the GPi control dyskinesia by activating inhibitory axons? Mov Disord. 2001; 16:208–16. [PubMed: 11295772]
124. Ashby P, Kim YJ, Kumar R, Lang AE, Lozano AM. Neurophysiological effects of stimulation through electrodes in the human subthalamic nucleus. Brain. 1999; 122:1919–31. [PubMed: 10506093]
125. Ashby P, Paradiso G, Saint-Cyr JA, Chen R, Lang AE, Lozano AM. Potentials recorded at the scalp by stimulation near the human subthalamic nucleus. Clin Neurophysiol. 2001; 112:431–7. [PubMed: 11222963]
126. Nowak LG, Bullier J. Axons, but not cell bodies, are activated by electrical stimulation in cortical gray matter II. Evidence from selective inactivation of cell bodies and axon initial segments. Exp Brain Res. 1998; 118:489–500. [PubMed: 9504844]
127. McIntyre C. Brief thoughts on ECT parameter settings. Brain Stimul. 2008; 1:88. [PubMed: 20633374]
128. André V, Henry D, Nehlig A. Dynamic variations of local cerebral blood flow in maximal electroshock seizures in the rat. Epilepsia. 2002; 43:1120–8. [PubMed: 12366724]

129. Engel JJ, Kuhl DE, Phelps ME. Patterns of human local cerebral glucose metabolism during epileptic seizures. Science. 1982; 218:64–6. [PubMed: 6981843]

130. McCown TJ, Duncan GE, Johnson KB, Breese GR. Metabolic and functional mapping of the neural network subserving inferior collicular seizure generalization. Brain Res. 1995; 701:117–28. [PubMed: 8925273]

131. Blumenfeld H, McNally KA, Ostroff RB, Zubal IG. Targeted prefrontal cortical activation with bifrontal ECT. Psychiatry Res. 2003; 123:165–70. [PubMed: 12928104]

132. Blumenfeld H, Westerveld M, Ostroff RB, Vanderhill SD, Freeman J, Necochea A, Uranga P, Tanhehco T, Smith A, Seibyl JP, Stokking R, Studholme C, Spencer SS, Zubal IG. Selective frontal, parietal, and temporal networks in generalized seizures. NeuroImage. 2003; 19:1556–66. [PubMed: 12948711]

133. Enev M, McNally KA, Varghese G, Zubal IG, Ostroff RB, Blumenfeld H. Imaging onset and propagation of ECT-induced seizures. Epilepsia. 2007; 48:238–44. [PubMed: 17295616]

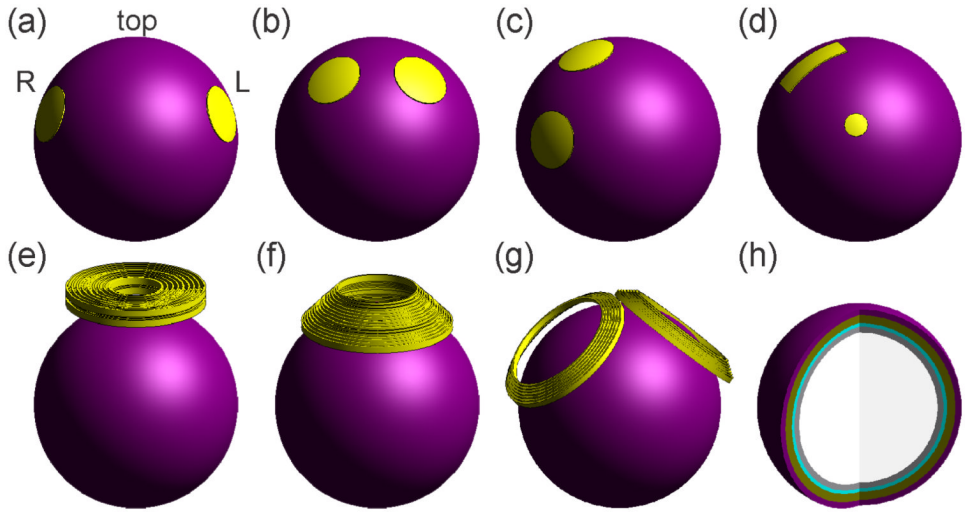

Figure 1.

Simulation models of ECT electrode and MST coil configurations: (a) bilateral (BL) ECT, (b) bifrontal (BF) ECT, (c) right unilateral (RUL) ECT, (d) focal electrically administered seizure therapy (FEAST), (e) circular coil (CIRC) MST, (f) cap coil (CAP) MST, (g) double-cone coil (DCONE) MST, and (h) interior of the five-layer spherical head model. Tissue layers from outer to inner shell: scalp, skull, cerebrospinal fluid, gray matter, and white matter.

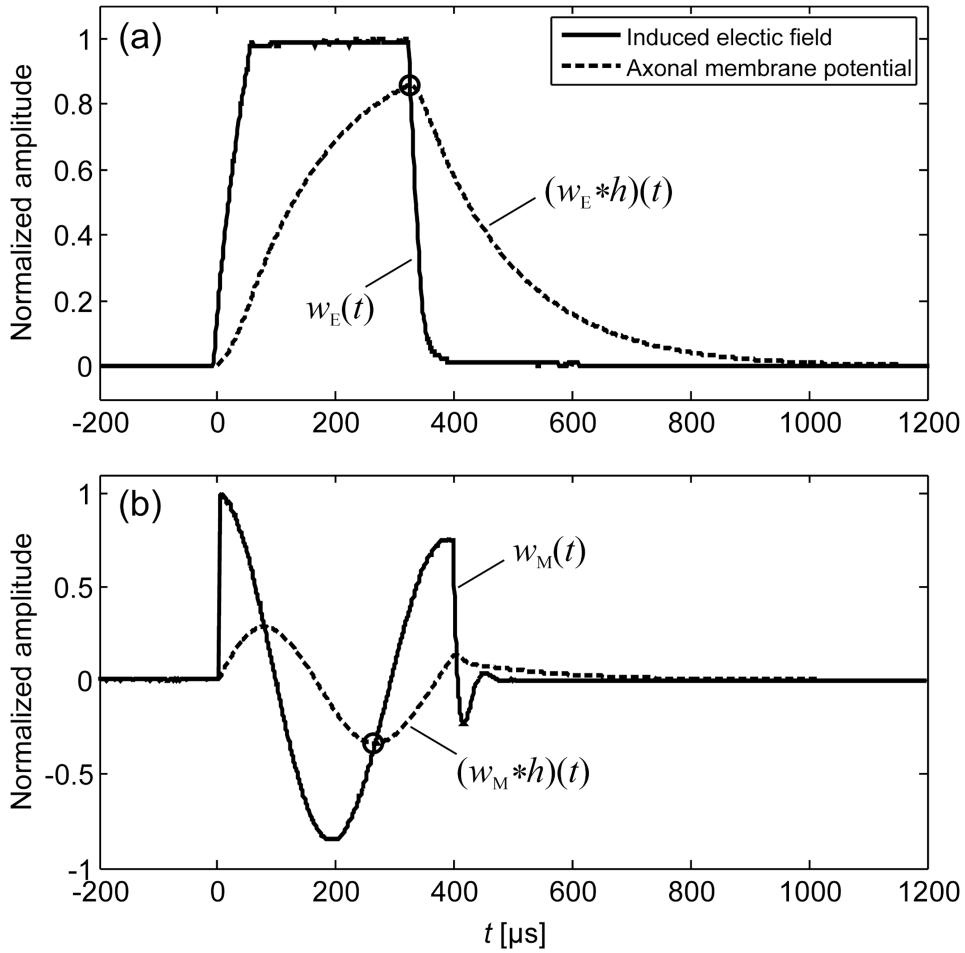

Figure 2.

Recorded electric field waveforms and estimated axonal membrane potentials for (a) ECT (0.3 ms pulse width) and (b) MST (CIRC coil). The peaks of the pulse waveforms were normalized to unity. The circles mark the peak change in axonal membrane potential.

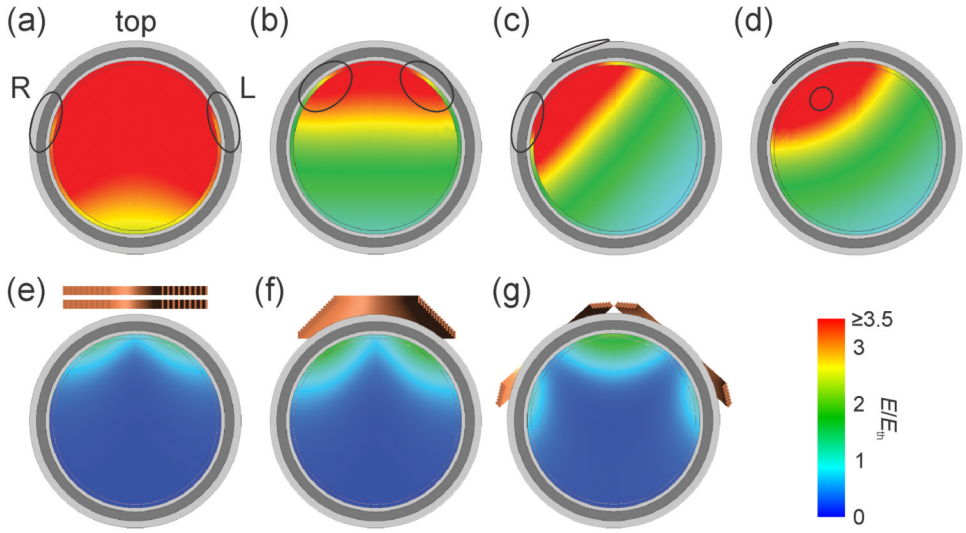

Figure 3.

Electric field strength relative to neural activation threshold for (a) BL ECT, (b) BF ECT, (c) RUL ECT, (d) FEAST, (e) CIRC MST, (f) CAP MST, and (g) DCONE MST. Coronal view from location immediately posterior to the bifrontotemporal electrodes in BL ECT. The outlines in (a)–(d) show the projected locations of the electrodes. ECT pulse width is 0.3 ms.

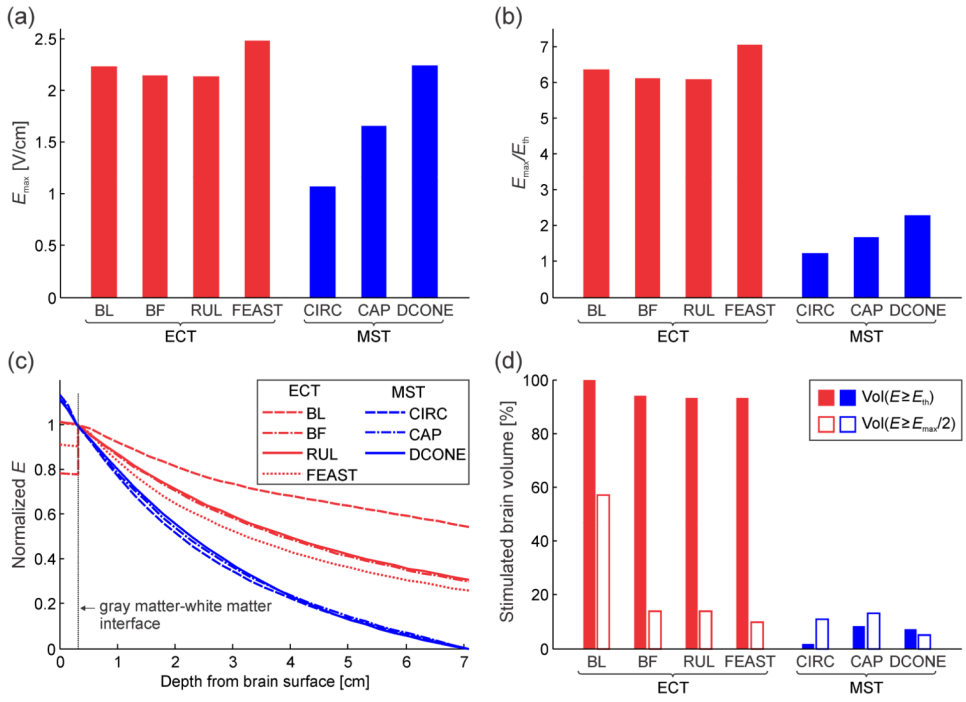

Figure 4.

Electric field characteristics: (a) maximum electric field, E_{max}, (b) maximum electric field relative to neural activation threshold, E_{max}/E_{th}, (c) electric field as a function of depth in the brain from the gray matter surface (the electric field magnitude is normalized to unity at the gray matter-white matter interface), and (d) directly activated brain volume, Vol($E \geq E_{th}$), and percentage of brain volume that is exposed to electric field larger than half-maximum, Vol($E \geq E_{max}/2$). ECT E_{th} is for pulse width of 0.3 ms.

Table 1

Head model parameters.

Tissue	Thickness (mm)	Conductivity (S/m)
Scalp	5.60	0.33
Skull	7.08	0.0083
Cerebrospinal fluid	3.00	1.79
Gray matter	3.00	0.33
White matter	67.8	0.14

Table 2

Estimated neural membrane depolarization factor, $\max(|(w * h)(t)|)$, and neural activation threshold, E_{th}.

Configurations	$\max(\|(w * h)(t)\|)$	E_{th} (V/cm)
TMS, Figure 8 coil	0.25	1.19*
ECT, 1 ms pulse width	0.99	0.30
ECT, 0.3 ms pulse width	0.86	0.35
CIRC MST	0.34	0.89
CAP MST	0.30	0.99
DCONE MST	0.30	1.00

* Empirically determined 1.4 × average threshold in motor cortex.